

# Field Programmable Gate Array-Based Attitude Stabilization

Michael J. Stepaniak,\* Maarten Uijt de Haag,<sup>†</sup> and Frank van Graas<sup>‡</sup>

*Avionics Engineering Center, Ohio University, Athens, OH 45701*

A system for determining vehicle attitude using a field programmable gate array (FPGA) and low cost gyroscopes is presented. The method is intended to support the stabilization of a short duration, unmanned aerial vehicle. Using a microelectromechanical system (MEMS) inertial sensor for the calibration and serial interface, the algorithm sidesteps concerns related to electromagnetic interference and the impact of embedded, proprietary filters. An Allan variance analysis is used to characterize the sensor errors and predict system performance. A floating point representation using a direction cosine matrix is hosted on the FPGA alongside the platform stabilization feedback loops. Although prone to drifting without additional aiding, the derived attitude has been demonstrated to be effective in stabilizing a remotely piloted quadrotor.

## Nomenclature

$f$	frequency
$A$	angle random walk
$b_i$	bit length of the initialization period
$B$	bias instability
$C$	attitude direction cosine matrix
$f$	sensor data rate
$I$	identity matrix
$K$	number of intervals
$M$	number of samples per interval
$T_i$	initialization period

---

\*Ph.D. Candidate, Avionics Engineering Center, Ohio University, AIAA Member

<sup>†</sup>Professor, Avionics Engineering Center, Ohio University, AIAA Member

<sup>‡</sup>Professor, Avionics Engineering Center, Ohio University

## Report Documentation Page

*Form Approved*  
*OMB No. 0704-0188*

Public reporting burden for the collection of information is estimated to average 1 hour per response, including the time for reviewing instructions, searching existing data sources, gathering and maintaining the data needed, and completing and reviewing the collection of information. Send comments regarding this burden estimate or any other aspect of this collection of information, including suggestions for reducing this burden, to Washington Headquarters Services, Directorate for Information Operations and Reports, 1215 Jefferson Davis Highway, Suite 1204, Arlington VA 22202-4302. Respondents should be aware that notwithstanding any other provision of law, no person shall be subject to a penalty for failing to comply with a collection of information if it does not display a currently valid OMB control number.

1. REPORT DATE <b>01 JUL 2008</b>	2. REPORT TYPE <b>N/A</b>	3. DATES COVERED <b>-</b>			
4. TITLE AND SUBTITLE <b>Field Programmable Gate Array-Based Attitude Stabilization</b>		5a. CONTRACT NUMBER			
		5b. GRANT NUMBER			
		5c. PROGRAM ELEMENT NUMBER			
6. AUTHOR(S)		5d. PROJECT NUMBER			
		5e. TASK NUMBER			
		5f. WORK UNIT NUMBER			
7. PERFORMING ORGANIZATION NAME(S) AND ADDRESS(ES) <b>Avionics Engineering Center, Ohio University, Athens, OH 45701</b>		8. PERFORMING ORGANIZATION REPORT NUMBER			
9. SPONSORING/MONITORING AGENCY NAME(S) AND ADDRESS(ES) <b>AFIT/ENEL Wright-Patterson AFB OH 45433-7765</b>		10. SPONSOR/MONITOR'S ACRONYM(S)			
		11. SPONSOR/MONITOR'S REPORT NUMBER(S) <b>CI09-0009</b>			
12. DISTRIBUTION/AVAILABILITY STATEMENT <b>Approved for public release, distribution unlimited</b>					
13. SUPPLEMENTARY NOTES					
14. ABSTRACT					
15. SUBJECT TERMS					
16. SECURITY CLASSIFICATION OF:			17. LIMITATION OF ABSTRACT <b>UU</b>	18. NUMBER OF PAGES <b>15</b>	19a. NAME OF RESPONSIBLE PERSON
a. REPORT <b>unclassified</b>	b. ABSTRACT <b>unclassified</b>	c. THIS PAGE <b>unclassified</b>			

$\theta$	pitch angle
$\phi$	roll angle
$\psi$	yaw angle
$\sigma_A^2$	Allan variance
$\tau_M$	period spanning M samples
$\Theta_{\times}$	skew-symmetric form of the angle vector
$\bar{\omega}_k$	mean angular rate for interval k
$\omega$	angular rate vector
$\omega_{arw}$	angular rate due to angle random walk
$\omega_{bi}$	angular rate due to bias instability
$\Omega_{\times}$	skew-symmetric form of the angular rate vector

*Subscript*

$r$	command reference
$x$	body $x$ -axis, aligned with a motor arm
$y$	body $y$ -axis, aligned with an orthogonal arm
$z$	body $z$ -axis, oriented down

## Introduction

The Avionics Engineering Center (AEC) at Ohio University has designed a quadrotor unmanned aerial vehicle for use as a sensor testbed platform. With the sensor payload rigidly attached to the airframe, as shown in Fig. 1, platform stabilization is required to position and orient the vehicle for sensor targeting. Stability augmentation can be accomplished using simple classical control techniques if both the attitude angles and angular rates are available. Although commercial autopilots are available that provide this data, they rely on the Global Positioning System (GPS)<sup>1</sup> and are therefore not suitable for AEC research involving GPS-denied environments.

However, a low-cost inertial system can be effectively applied since the vehicle will be piloted remotely. Combining gyroscopes with accelerometers and magnetometers provides reasonable accuracy, but these microelectromechanical system (MEMS) sensors are both susceptible to electromagnetic interference and introduce an element of uncertainty due to proprietary blending algorithms. Therefore, this paper investigates the ability to derive a satisfactory attitude solution using only the gyroscope data from a MEMS inertial sensor. The remainder of this paper characterizes the Microstrain 3DM-GX1, presents the algorithm for propagating attitude over time, describes the implementation in a field programmable gate array (FPGA),



**Figure 1. AEC Quadrotor**

and concludes with flight test results.

## Background

The Microstrain 3DM-GX1, Fig. 2, is a MEMS inertial unit capable of providing orientation information using an RS-232 serial port. The attitude solution benefits greatly from the application of a proprietary algorithm that blends the output of orthogonal gyroscopes with data from the accelerometers and magnetometers in order to minimize drift and sensitivity to inertial forces. For dynamic applications, the 3DM-GX1 reportedly provides 2 degree RMS accuracy typical.<sup>2</sup> The level of performance, combined with a relatively low cost, makes devices such as these well-suited for unmanned vehicles applications especially when aided by the global positioning system.<sup>3-5</sup> In addition, without aiding, the 3DM-GX1 has previously been demonstrated capable of hovering a micro air vehicle autonomously for 35 seconds and for several minutes when assisting a pilot.<sup>6</sup>



**Figure 2. Microstrain 3DM-GX1 Orientation Sensor**

One limitation of the 3DM-GX1 is the sensitivity of the unit's magnetometers to electromagnetic interference and the presence of metal objects. In fact, the magnetic disturbances measured by the 3DM-GX1 have been used as an additional means of positioning.<sup>7</sup> Potential sources of interference on the AEC quadrotor include four high power motors, with motor currents as high as 55 amps each, the avionics associated with the flight control system, and possibly the sensor payload as well. One means of mitigating the errors on the blended navigation solution used for wheeled robots is to position the sensor as far as possible from the sources of interference.<sup>8</sup> Within the constraints of a small aerial vehicle, an alternate solution is to limit

aiding performed by the the magnetometers. For example, German researchers integrating a GPS receiver with a MEMS inertial measurement unit opted to restrict the magnetometers aiding to the yaw channel only where errors such as 20 degrees were considered “tolerable”.<sup>4</sup>

In addition to interference, the filtering itself can add undesired artifacts. For example, the low pass filter used in the blending algorithm is susceptible to “sustained inertial influences”.<sup>9</sup> Also, the filter adds unspecified phase lag which has a destabilizing effect. To mitigate the interference and eliminate uncertainty associated with a proprietary algorithm, the proposed solution is to bypass the proprietary filters altogether and to perform bias-compensation and the attitude calculation externally on a field programmable gate array (FPGA). This approach relies solely on the gyroscopes for inertial data, minimizing the impact of electromagnetic interference, and allows implementation on a single light-weight board which is capable of hosting both the attitude algorithm and the flight control system. The remaining sections in this paper detail the implementation of the attitude algorithm, characterize the performance, and present the results noted during flight test of the AEC quadrotor sensor testbed.

Without requiring data from the accelerometers and magnetometers, only a portion of the functionality of the 3DM-GX1 was utilized. As such, this technique described in this paper could also be applied to discrete microelectromechanical system (MEMS) gyroscopes. However, the 3DM-GX1 sensor package was retained to take advantage of the digital interface and the gyroscope calibration. The “instantaneous” angular rate vector, to which blending has not been applied, is compensated for temperature, alignment, and G-sensitivity but not for the constant bias.<sup>10</sup>

A byproduct of bypassing the internal bias compensation algorithm is an increase in maximum data rate for Euler angles from 100 Hz to 333 Hz.<sup>11</sup> The increased data rate benefits the fidelity of the attitude solution, though the control loop for the quadrotor is still constrained to 50 Hz by the pulse width modulated protocol used by the radio receiver and electronic speed controllers.

## Allan Variance Analysis

The instantaneous angular rates retain a significant bias that can be removed by averaging the angular rate during an initialization period and then subtracting this bias from subsequent measurements. The appropriate averaging interval is determined from a plot of the Allan variance versus averaging interval. The Allan variance provides the variation between mean values calculated for consecutive intervals and is calculated as<sup>12</sup>

$$\sigma_A^2(\tau_M) = \frac{1}{2(K-1)} \sum_{k=1}^{K-1} (\bar{\omega}_{k+1}(M) - \bar{\omega}_k(M))^2 \quad (1)$$

where  $N$  is the total number of data points,  $M$  is the number of sample points in an interval, and  $K = \text{floor}(N/M)$  is the integer number of distinct intervals that can be formed within the collected data.

With data collected at a constant frequency,  $f$ , the length of the interval is given by  $\tau_M = M/f$ . The mean value of the  $k^{\text{th}}$  interval is denoted by  $\bar{\omega}_k$ .

The percent error associated with the root Allan Variance, or Allan standard deviation, is given by<sup>12</sup>

$$\% \text{ error} = \frac{100}{\sqrt{2(K-1)}} \quad (2)$$

Because the percent error grows rapidly as the interval length approaches the sample length, care must be taken to collect sufficient data to avoid erroneous results. The data set represented in Fig. 3 was collected at 333 Hz for 6.7 hours in order and exhibits less than ten percent error for averaging intervals under eight minutes in length. The minimum point for each curve indicates the interval length for which the calculated mean will remove the bias with minimal residual error. Although the three gyros attained minimum variance at different interval lengths, for simplicity a single initialization period of 50 seconds was selected for all three gyros.

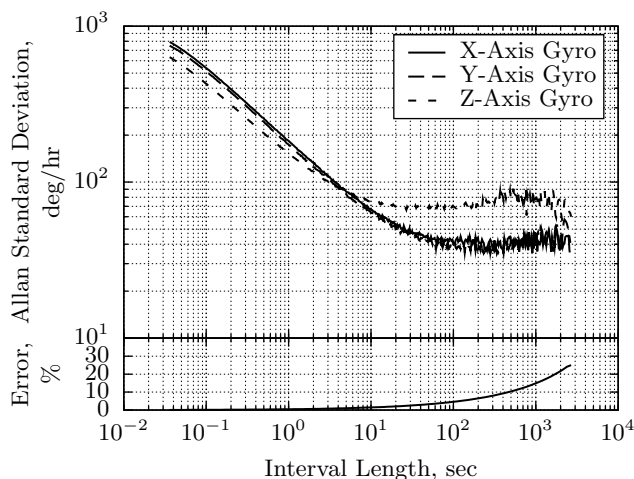


**Figure 3. Allan Variance Plot for the Gyroscopes**

The Allan variance analysis also provides a graphical method for estimating sensor noise based on the slopes of various line segments as detailed in references 12 and 13. In particular for the quadrotor, the  $-\frac{1}{2}$  slope for short averaging intervals is indicative of angle random walk and level segment for larger intervals is associated with the bias instability. The following expression for angle random walk,  $A$ , adds a conversion factor of  $1/3600$  to the expression typically used<sup>12</sup> allowing the formula to be applied to the curve as depicted without having to extrapolate the sloped line to an intercept at  $\tau = 3600$  seconds.

$$A = \sigma_A \frac{\sqrt{\tau}}{60} \quad (3)$$

As an example, for the x-axis gyroscope shown in Fig. 3, the standard deviation for a 0.85 sec interval is

200 deg/hr corresponding to a angle random walk of 3.1 deg/ $\sqrt{\text{hr}}$ . The bias instability coefficient,  $B$ , is proportional to Allan standard deviation of the horizontal segment<sup>12</sup>

$$B = \sigma_A \sqrt{\frac{\pi}{2 \ln 2}} \quad (4)$$

The noise coefficients extracted from the Allan variance analysis are listed in Table 1 for each of the three gyroscopes. The measured coefficients are found to be in reasonable agreement with the manufacturer provided specifications though the z-axis gyroscope exhibits a larger than expected bias instability.

**Table 1. Allan Variance-Derived Noise Coefficients**

Noise Source (units)	Spec.	Value	
Angle Random Walk ( $\frac{\text{deg}}{\sqrt{\text{hr}}}$ )	3.5	x-axis	3.1
		y-axis	2.9
		z-axis	2.6
Bias Instability ( $\frac{\text{deg}}{\text{hr}}$ )	72	x-axis	61
		y-axis	56
		z-axis	104

## Deriving Attitude

The platform attitude is the orientation of a body fixed reference system to inertial space. The body reference frame, Fig. 4, is defined analogous to the typical fixed wing aircraft with the origin located at the center of gravity, the  $x$ -axis is aligned with one arm, the  $z$ -axis pointing down, and the  $y$ -axis aligned with a second arm consistent with a right-hand coordinate system. For the short duration flights planned, the rotation of the earth can be ignored and the axes of the inertial reference frame set to North, East, and Down.

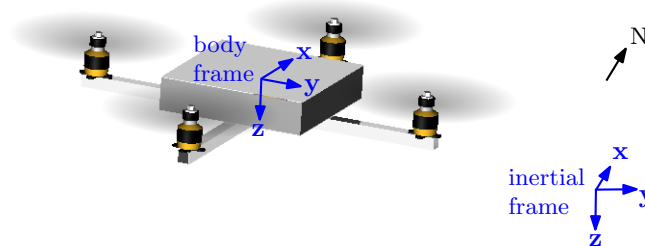


**Figure 4. Quadrotor Reference Frames**

The attitude is described by three Euler angles,  $\psi$ ,  $\theta$ , and  $\phi$ . Applying the *yaw-pitch-roll* convention, the Euler angles describe three successive rotations about the body  $z$ -,  $y$ - and  $x$ -axes. In general the Euler angles are not functions of the body axis angular rates, but rather of angular rates about intermediate axis.

Therefore, the body angular rates measured by a strapdown inertial unit cannot be directly integrated to generate the Euler angles. Instead, the attitude is propagated using a direction cosine matrix from which the Euler angles can be extracted as needed. The direction cosine matrix relating the body and inertial frames using the Euler angles is<sup>14,15</sup>

$$\mathbf{C} = \begin{bmatrix} \cos \theta \cos \psi & -\cos \theta \sin \psi + \sin \phi \sin \theta \cos \psi & \sin \phi \sin \psi + \cos \phi \sin \theta \cos \psi \\ \cos \theta \sin \psi & \cos \theta \cos \psi + \sin \phi \sin \theta \sin \psi & -\sin \phi \cos \psi + \cos \phi \sin \theta \sin \psi \\ -\sin \theta & \sin \phi \cos \theta & \cos \phi \cos \theta \end{bmatrix} \quad (5)$$

This matrix is propagated forward in time using<sup>14</sup>

$$\dot{\mathbf{C}} = \mathbf{C}\boldsymbol{\Omega}_{\times} \quad (6)$$

where  $\boldsymbol{\Omega}_{\times}$  is the skew-symmetric form of the body angular rate vector measured by the gyroscopes

$$\boldsymbol{\Omega}_{\times} = \begin{bmatrix} 0 & -\omega_z & \omega_y \\ \omega_z & 0 & -\omega_x \\ -\omega_y & \omega_x & 0 \end{bmatrix} \quad (7)$$

Because the gyroscopes' data rate is high compared to the bandwidth for the quadrotor platform, a first-order approximation is sufficient to propagate the attitude direction cosine matrix in discrete time

$$\mathbf{C}_{k+1} = \mathbf{C}_k e^{\boldsymbol{\Omega}_{\times}} \approx \mathbf{C}_k (\mathbf{I} + \boldsymbol{\Theta}_{\times}) \quad (8)$$

The Euler angles can be extracted from the direction cosine matrix using trigonometry:

$$\begin{aligned} \phi &= \arctan \frac{\mathbf{C}(3,2)}{\mathbf{C}(3,3)} \\ \theta &= -\arcsin \mathbf{C}(3,1) \\ \psi &= \arctan \frac{\mathbf{C}(2,1)}{\mathbf{C}(1,1)} \end{aligned} \quad (9)$$

## Hardware Implementation

The quadrotor's flight control system is implemented in a Xilinx Spartan-3 field programmable gate array (FPGA) hosted on a Digilent starter board. The size and weight of the FPGA board are suitable for use on the moderate-sized quadrotor platform. In addition, the starter board provides a serial port for interfacing with the inertial sensor and also sufficient switches and displays to facilitate setting options and reporting

system status. The attitude algorithm is hosted on a one million gate FPGA with a system clock operating at 50 MHz. To accommodate additional planned functionality, the footprint of the attitude algorithm was minimized where possible. A block diagram of the system is shown in Fig. 5.

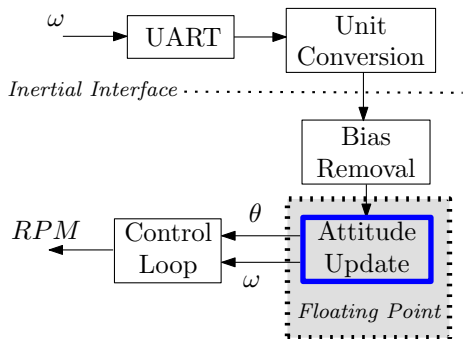


**Figure 5. FPGA Block Diagram**

### Inertial Interface

A generic signal interface for the inertial sensor was established to facilitate the use of other sensors in the future. This interface consists of the following five signals: angular rate measurements for three axes in rad/sec, the time increment in seconds since the last data set, and a boolean flag that is asserted when a new data set is ready. Specifically for the Microstrain 3DM-GX1, the FPGA establishes serial port communications, places the sensor into a continuous data transfer mode, performs basic error checking, and then, because the Microstrain provides angular rates and time increments in 16-bit raw counts, provides signal conversion.

The scale factor for angular rate,  $17 \times 2^{-16}$  is readily implemented in fixed point arithmetic using a simple multiplication followed by a shift operation. The time scale factor,  $0.003 = \frac{3}{125} \times 2^{-3}$ , however, cannot be implemented without introducing rounding error. As shown in Table 2 selecting a scale factor word length of ten bits or greater minimizes the degradation in accuracy.

**Table 2. Rounding Error in the Time Scale Factor**

Length (bits)	Value (ms)	Error (%)
8, 9	3.91	30.21
10–12	2.93	2.34
13	3.05	1.73
14, 15	2.99	0.31
16	3.01	0.20

## Bias Compensation

The nominal 50 minute initialization period,  $T_i$ , used to determine the sensor bias is adjusted so that the mean can be implemented in hardware by a summation followed by a simple shift operation. Because the Allan variance analysis exhibited a flat bias instability region for the interval of interest, a slight increase in the initialization period is of no consequence.

If  $f$  is the sensor data rate and  $T_i$  is the initialization period, then the modified initialization period is given by

$$T'_i = \frac{2^{b_i}}{f} \quad (10)$$

where  $b_i = \text{ceil}(\log_2(T_i f))$  and the  $\text{ceil}()$  operator rounds up to the next integer. The number of samples to be included in the summation is  $2^{b_i}$  and decimal is shifted over  $b_i$  bits to calculate the mean. For precision, the bias and the corrected angular rates retain all fractional bits.

## Radio Receiver Interface

Even after removing the initial bias, the bias instability and the angle random walk in the sensor will introduce a residual nonstationary error that must be manually compensated for by the pilot. With stick inputs that only cover a fixed range, the scale factor for the reference command inputs must be applied in the FPGA that is large enough to accommodate predicted error growth without unduly raising the system gain. In practice, without additional aiding the error grows without bounds and the flight ends when a full stick input is required to maintain a level attitude.

Neglecting the coupling inherent in the Euler angles, the attitude angles can be represented in a simple form as

$$\Theta = \int \omega_t dt \quad (11)$$

As shown in the Allan variance analysis, the angular rate is corrupted by errors due to bias instability and angle random walk such that  $\omega = \omega_t + \omega_{arw} + \omega_{bi}$ . In addition, the time interval contains a scaling error caused by rounding,  $t = t_t(1 + S_r)$ . Incorporating these errors the expression for attitude is

$$\begin{aligned} \Theta &= \int (\omega_t + \omega_{arw} + \omega_{bi}) d(t_t(1 + S_r)) \\ &= \int (\omega_t(1 + S_r) + (\omega_{arw} + \omega_{bi})(1 + S_r)) dt_t \\ &= \Theta_t(1 + S_r) + \int (\omega_{arw} + \omega_{bi})(1 + S_r) dt_t \end{aligned} \quad (12)$$

where the first term represents a scaling of the true attitude and the second term is the error due to both sensor noise and rounding error. Since the quadrotor flight profile that consists of only nominal excursions

from a hover, the true attitude will generally remain close to zero for pitch and roll and the affect of rounding is minimal. The second term is the residual error for which the pilot must compensate. The uncertainty of this term as a function of time is

$$\sigma_{\Theta}(t) = (A\sqrt{t} + Bt)(1 + S_r) \quad (13)$$

Using the error coefficients from Table 1 and a 10-bit time scale factor, a suitable command reference scale factor can be selected that encompasses the two-sigma attitude uncertainties for roll and pitch angles. For example, from Fig. 6 a scale factor corresponding to  $\pm 13$  degrees accommodates five minutes of flight. This duration is sufficient for many of the profiles planned for the AEC quadrotor and longer flights are accommodating by increasing the scale factor at the expense of increasing the sensitivity to the control stick.

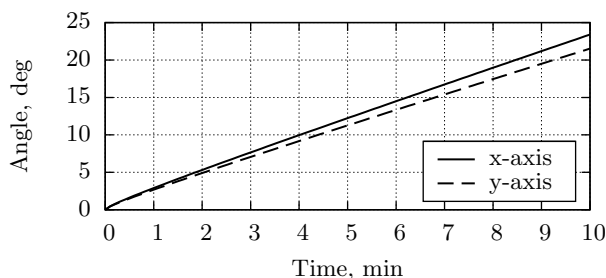


**Figure 6. Uncertainty ( $2\sigma$ ) in Roll and Pitch**

### Calculating Attitude

Based on resolution, the sensor was capable of reporting an incremental angular change as small as 0.78 microradians. To adequately cover the dynamic range from the incremental change to a full rotation, a floating point representation was implemented for the attitude calculations. The exponent was set at six bits to span the dynamic range and length of the mantissa was determined using a simulation of the FPGA algorithm. The algorithm was propagated using a brief data set collected as the inertial sensor was subjected to a series of doublets followed by a three-axis oscillation. The length of the mantissa was then set at 18 bits, the level beyond which the improvement in accuracy was negligible, as seen in Fig. 7 which is a representative plot of the roll angle error.

A direct coding of the 3x3 matrix multiplication is impractical based on the requirement for 18 additions and 27 products. The resources required for these operations is summarized in Table 3 in terms of slices, each of which contains two four-input lookup tables and two flip-flops, and dedicated 18x18 multipliers. The Spartan-3 chip used contains 7680 slices and 24 dedicated multipliers. For comparison, the results for a 25 bit fixed point implementation is also included. While the products can be readily implemented, and are in fact more compact than the corresponding fixed point representation, the floating point addition is prohibitively large. Therefore, the matrix multiplication is subdivided first into a series of dot products and then into

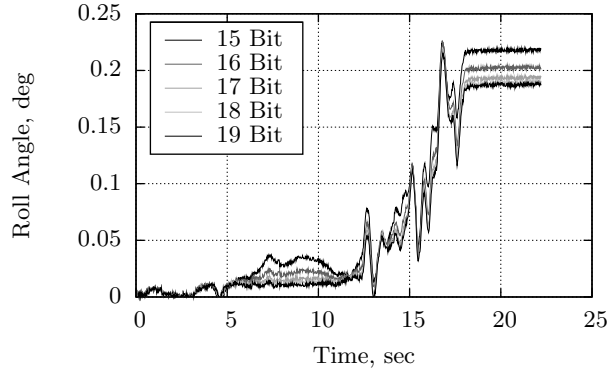


**Figure 7. Roll Angle Error with Varying Mantissa Length**

a series of additions, each of which is carried out sequentially using the same hardware. As implemented the matrix multiplication occupies 1191 slices and 3 multipliers, corresponding to 15% and 12% of available resources, respectively.

**Table 3. Floating Point vs Fixed Point Operations**

Operation	Type	Slices	18x18 Multipliers	Latency (ns)
Addition	Float	421	0	14.3
	Fixed	27	0	7.0
Multiplication	Float	51	1	15.1
	Fixed	53	4	15.6

The pitch and roll angles required for platform stabilization are extracted from the direction cosine matrix using small angle approximations and Equation (9). Note that the small angle approximations impact only the pitch and roll angles calculated for a specific moment in time and have no influence on the accuracy of the attitude solution carried in the direction cosine matrix, even in the case of large excursions in pitch or roll. For the quadrotor platform, pitch and roll angles are controlled to be less than eight degrees and the heading maintained solely by the pilot so the minimal errors introduced are inconsequential. For other applications it may be beneficial to implement the trigonometric functions using the coordinate rotation digital computer (CORDIC) algorithm or lookup tables.

### Control Loop

The flight control system used feedback loops, shown in Fig. 8, to stabilize the vehicle based on the measured angular rate and the derived attitude angles. Note that with symmetry the feedback loops for the roll channel are identical to that for the pitch channel. Feedback gains and the lead compensator were initially selected to achieve desired performance and then the values were adjusted to be of the form  $K = \alpha \times 2^\beta$ .

This facilitated implementation on the FPGA in a fixed point notation using only multipliers and shift operations. Performance with the new gains was then then verified to ensure that the desired performance was not adversely impacted.

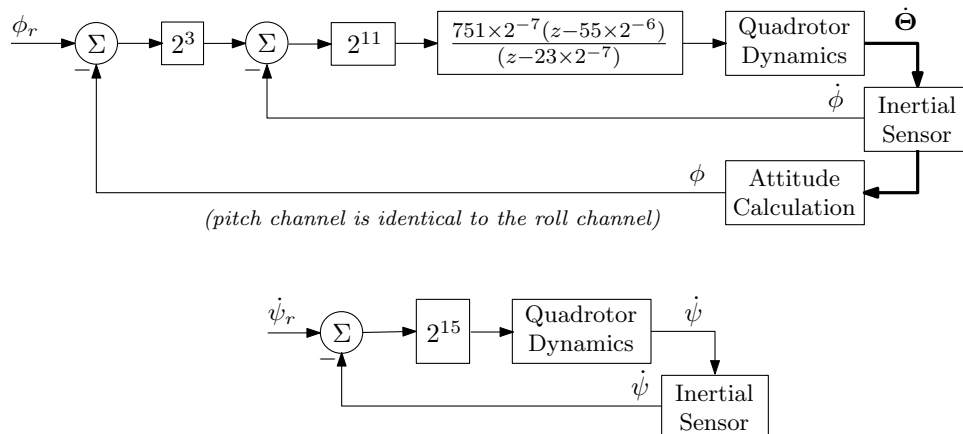


**Figure 8. Flight Control System Diagram**

The quadrotor dynamics include the motor and propeller as well as the aerodynamics. The input quadrotor dynamics is a pulse width modulated (PWM) motor command signal that is delivered to an electronic speed controller. The standard PWM signals used for the quadrotor have a variable width component of 0-1 ms. With the FPGA operating at 50 MHz, the PWM interface is able to provide a command signal resolution of 1/50,000. The ability of the speed controller to respond to 20 ns changes was not ascertained and likely varies between different models. Nonetheless, an upper bound on the useful resolution of the attitude signals is determined the closed loop gain which varies as a function of the PWM resolution. With the closed loop gains shown in Fig. 8, angular precision, in radians, beyond 14 bits will have no impact on the motor commands. This equates to an effective resolution of  $3.5 \times 10^{-3}$  degrees compared to the sensor resolution of  $4.5 \times 10^{-5}$  degrees.

## Results

A Monte Carlo analysis confirms that measured data matches the error model described by Equation (13), validating the use of the Allan variance to estimate noise coefficients. Fig. 9 shows the roll angle Monte Carlo plot and the predicted and calculated statistics. The pitch axis exhibits similar characteristics with yaw axis having somewhat worse performance as anticipated by the noise coefficients in Table 1. The data were collected from a stationary sensor and the Euler angles were calculated using the FPGA algorithm after compensating for the bias from the angular rates as previously described. As expected, there is significant error growth due to the bias instability even for short time periods.

Fig. 10 plots the standard deviation of the Monte Carlo analysis for each channel and the device's accuracy

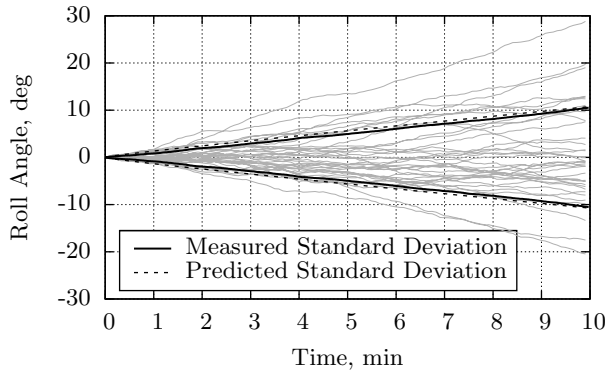


**Figure 9. Monte Carlo analysis (37 runs)**

specification for dynamic maneuvering. The dynamic accuracy was not measured due to limitations in data collection for the current quadrotor implementation. However, a Monte Carlo analysis for the static condition was completed and the one-sigma parameters were found to be in general agreement with the specifications:  $0.60^\circ$ ,  $0.56^\circ$ , and  $0.98^\circ$  for roll, pitch, and yaw, respectively compared to a specification of  $0.5^\circ$ . Furthermore, because the attitude algorithm is not based on the accelerometers, unlike the solution embedded in the sensor, the results are expected to be representative of dynamic performance.

Two conclusions can be drawn from Fig. 10. First, for the first two minutes the gyro-based solution implemented on the FPGA outperforms the dynamic-maneuvering specification. Second, the growth is slow enough that the drift can easily be correct for by the pilot. The operational limit for mission duration is then based on the scale factor applied to the command reference input. As long as the pilot can compensate for the drift using trim or manual inputs, the performance remains satisfactory.

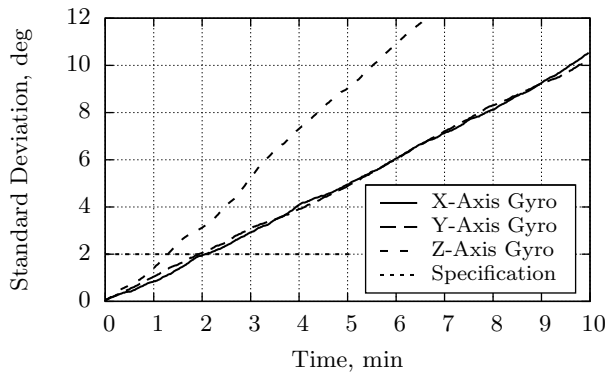


**Figure 10. Statistical Comparison of Attitude Methods**

Flight test results were consistent with predicted performance. With the FPGA providing stability augmentation, the operator was able to maintain a hover or maneuver the quadrotor without difficulty. Compensating for sensor drift using the trim switches on the radio controller was not practical, but compensating for the drift by holding a non-zero stick input was not problematic. Over time, the drift in attitude

would saturate one of the controls. However, it was not necessary to preemptively land as the drift was slow enough that the vehicle could still be brought down safely.

On two occasions the quadrotor lifted off with a slight pitch or roll rate. With velocity the double integral of the angle, this led to an unexpected translation and the operator opted to immediately land. The cause may be attributed to a chance offshoot in the angular rates, but with the data recording currently limited this could not be conclusively verified. The post-flight data did show a large bias in the indicated channel, but this could also have been the result of the hard landing saturating the gyroscope. In addition, the motors occasionally experience a brief jitter in power on the order of a second in duration. The attitude is largely unaffected, though there is an audible increase in motor speed, and no command inputs are necessary. Possibly a spike in the sensor noise is amplified by the lead compensator only to be immediately countered through the feedback loop. A data telemetry system is planned that will allow an analysis of both anomalies.

## Conclusions

The computational resources for the attitude algorithm can be easily implemented on a low-cost FPGA board. Even allowing for a floating point implementation and propagating the attitude using a direction cosine matrix, the FPGA board retains enough capacity to also host other functions including the control laws.

Although the results of the monte-carlo simulation show that the uncertainty in the attitude solution varies greatly over time, in flight test the variation has been shown to be manageable for profiles suitable for sensors research. The completion of the of a telemetry downlink will provide data to support a detailed analysis of anomalies noted and will also support the real-time evaluation of the sensor payload. Clearly some aiding will be necessary to provide an autonomous hover capability. However, for piloted flight, the excursions are small enough during the short battery-powered flights that the errors are not overly restrictive.

The views expressed in this article are those of the authors and do not reflect the official policy or position of the United States Air Force, the Department of Defense, or the United States Government.

## References

<sup>1</sup>Christophersen, H. B., Pickell, R., Neidhoefer, J. C., Koller, A. A., Suresh, K. K., and Johnson, E. N., "A Compact Guidance, Navigation, and Control System for Unmanned Aerial Vehicles," *Journal of Aerospace Computing, Information, and Communication*, Vol. 3, May 2006, pp. 187–213.

<sup>2</sup>Microstrain, Inc., Williston, VT, *Detailed Specifications for 3DM-GX1*, Retrieved May 28, 2008, [Available at [www.microstrain.com](http://www.microstrain.com)].

<sup>3</sup>Mancini, A., Caponetti, F., Monteriù, A., Frontoni, E., Zingaretti, P., and Longhi, S., "Safe Flying for an UAV Heli-

copter,” *Proceedings of the 15th Mediteranean Conference on Control & Automation*, Athens, Greece, July 27-29, 2007, pp. 1–6.

<sup>4</sup>Wendel, J., Meister, O., Schlaile, C., and Trommer, G. F., “An Integrated GPS/MEMS-IMU Navigation System for an Autonomous Helicopter,” *Aerospace Science and Technology*, Vol. 10, No. 6, Sept. 2006, pp. 527–533.

<sup>5</sup>Hoffmann, G. M., Huang, H., Waslander, S. L., and Tomlin, C. J., “Quadrotor Helicopter Flight Dynamics and Control: Theory and Experiment,” *AIAA Guidance, Navigation and Control Conference*, Aug. 20-23, 2007, pp. 1–20.

<sup>6</sup>Green, W. E. and Oh, P. Y., “Autonomous Hovering of a Fixed-Wing Micro Air Vehicle,” *Proceedings of the 2006 IEEE International Conference on Robotics and Automation*, Orlando, Florida, May 2006, pp. 2164–2169.

<sup>7</sup>Vissière, D., Martin, A., and Petit, N., “Using Magnetic Disturbances to Improve IMU-Based Position Estimation,” *Proceedings of the European Control Conference*, Kos, Greece, July 2–5, 2007, pp. 2853–2858.

<sup>8</sup>Cruz, D., McClintock, J., Perteet, B., Orqueda, O. A., Cao, U., and Fierro, R., “Decentralized Cooperative Control,” *IEEE Control Systems Magazine*, June 2007, pp. 58–78.

<sup>9</sup>Churchill, D. L. and Arms, S. W., *3DM-GX1 Gyro Enhanced Orientation Sensor FAQ’s*, Microstrain, Inc., Williston, VT, June 14, 2005, [Available at [www.microstrain.com](http://www.microstrain.com)].

<sup>10</sup>Microstrain, Inc., Williston, VT, *3DM-GX1 Data Communications Protocol, Version 3.1.00*, July 5, 2005, [Available at [www.microstrain.com](http://www.microstrain.com)].

<sup>11</sup>Microstrain, Inc., Williston, VT, *3DM-GX1 Orientation Sensor: Fastest Data Output Rates*, 2006, [Available at [www.microstrain.com](http://www.microstrain.com)].

<sup>12</sup>Ng, L. C. and Pines, D. J., “Characterization of Ring Laser Gyro Performance Using the Allan Variance Method,” *Journal of Guidance, Control, and Dynamics*, Vol. 20, No. 1, Jan-Feb 1997, pp. 211–214.

<sup>13</sup>El-Sheimy, N., Hou, H., and Niu, X., “Analysis and Modeling of Inertial Sensors Using Allan Variance,” *IEEE Transactions on Instrumentation and Measurements*, Vol. 57, No. 1, Jan. 2008, pp. 140–149.

<sup>14</sup>Titterton, D. H. and Weston, J. L., *Strapdown Inertial Navigation Technology*, Vol. 207 of *Progress in Astronautics and Aeronautics*, American Institute of Aeronautics and Astronautics, Inc., Reston, VA, 2nd ed., 2004.

<sup>15</sup>Nelson, R. C., *Flight Stability and Automatic Control*, McGraw-Hill, Inc., New York, 1989.